Journal of Catalysis **188,** 111–124 (1999)
Article ID jcat.1999.2663, available online at http://www.idealibrary.com on IDEAL®

Activity and Structure of Hydrotreating Ni, Mo, and Ni–Mo Sulfide Catalysts Supported on γ-Al_2O_3–USY Zeolite

Dien Li,*,†,[1] A. Nishijima,† D. E. Morris,‡ and G. D. Guthrie*

*Earth and Environmental Sciences Division and ‡Chemical Sciences and Technology Division, Los Alamos National Laboratory, Los Alamos, New Mexico 87545; and †Department of Surface Chemistry, National Institute of Materials and Chemical Research, Tsukuba, Ibaraki 305, Japan

Received March 16, 1999; revised July 16, 1999; accepted August 4, 1999

The catalytic hydrocracking (HC) of diphenylmethane (DPM) and hydrodesulfurization (HDS) of dibenzothiophene (DBT) over Ni, Mo, and Ni–Mo sulfide catalysts supported on a mixed ultrastable Y (USY) zeolite and γ-Al_2O_3 were studied. The catalysts were characterized using NH_3 temperature-programmed desorption (TPD), X-ray photoelectron spectroscopy (XPS), UV–Vis–NIR diffuse reflectance spectroscopy (DRS), high-resolution transmission electron microscopy (HRTEM), and chemical composition analysis. Because addition of zeolite to a conventional alumina support improves acidity, Ni, Mo, and Ni–Mo catalysts supported on the combined supports had much higher HC activity. Ni was found to be uniformly distributed throughout the catalysts; however, Mo preferentially entered the structure of γ-Al_2O_3 or was accommodated as oxide aggregates on γ-Al_2O_3, rather than associating with zeolite. Ni and Mo catalysts supported on γ-Al_2O_3–USY zeolite were good HDS catalysts and showed a shallow maximum in catalytic activity at a NiO and MoO_3 content of 5 mol%. The higher activity at this content occurred because Ni or Mo species had higher surface concentrations, higher dispersion, and were more easily sulfided. Ni–Mo catalysts supported on γ-Al_2O_3–USY zeolite had high HDS activity, which showed a prominent maximum at a NiO/(NiO + MoO_3) ratio of about 0.4, because at this ratio the surface species of Ni and Mo were well dispersed and more easily sulfided to form a Ni–Mo–S phase responsible for the high HDS activity. The Ni–Mo catalysts supported on γ-Al_2O_3–USY zeolite have slightly higher HDS activity than γ-Al_2O_3-supported Ni–Mo catalysts.

Key Words: **Ni–Mo/γ-Al_2O_3–USY zeolite; hydrocracking; hydrodesulfurization; NH_3 temperature-programmed desorption; X-ray photoelectron spectroscopy; diffuse reflectance spectroscopy.**

INTRODUCTION

Mo and W sulfide catalysts supported on γ-Al_2O_3 and promoted by Co and Ni have been applied to the industrial hydrotreatment of petroleum and liquefied coal (1). However, new environmental regulations require that the sulfur content in diesel fuel be significantly reduced to less than 0.05 wt%, which is not currently achievable with the γ-Al_2O_3-based catalysts. The major sulfur-containing compounds in diesel fuel are benzothiophene, dibenzothiophene (DBT), 4-methyldibenzothiophene, and 4,6-dimethyldibenzothiophene. It is well known that the hydrodesulfurization (HDS) of DBT compounds proceeds by two processes: hydrogenation (HYD) of the DBT ring and hydrocracking (HC) of S–C bonds. Alumina-supported transition metal sulfide catalysts have a high HYD activity but a relatively poor HC activity in hydrotreating processes. In contrast, zeolites have a very high HC activity (2), but their catalytic activity is easily deactivated under hydrotreating conditions. Thus, one potential class of efficient next-generation HDS catalysts appears to be the combination of Ni–Mo/γ-Al_2O_3 with zeolites, which would result in both high HYD and HC activities and greater accessibility of DBT molecules to the active sites.

Several studies have found that a combination of Ni–Mo sulfide catalyst with zeolites is a promising approach to next-generation hydrotreating catalysts. Mann *et al.* (3) studied the HDS and hydrodenitrogenation (HDN) of heavy gas oil over Ni–Mo sulfide catalysts supported on zeolite–alumina–silica at 350–425°C, and they found that this combination of catalysts can remove as much as 99% S and 86% N at 425°C. Harvey and Pratt (4) studied the HDN reaction of quinoline over catalysts of metal ion-exchanged Y zeolite mixed with a standard Ni–Mo/γ-Al_2O_3 and found that only ruthenium-exchanged Y zeolite promotes the HDN activity of the standard Ni–Mo/γ-Al_2O_3 catalyst. Shimada *et al.* (5) compared the catalytic activities of coal-derived liquids over a series of Ni–Mo/γ-Al_2O_3–HY zeolite catalysts. They found that HYD activity decreases and HC activity increases with the proportion of Y zeolite in the support and that the HDN and HYD activities of the zeolite-supported catalysts are generally poorer than those of alumina-supported catalysts. Minja and Ternan (6) found that the addition of H-mordenite to a Co–Mo/γ-Al_2O_3 catalyst can increase V and Ni hydrodemetallization,

[1] To whom correspondence should be addressed at EES-1, MS D462, Earth and Environmental Sciences Division, Los Alamos National Laboratory, Los Alamos, NM 87545. Fax: (505) 665–3285. E-mail: dienli@lanl.gov.

0021-9517/99 $30.00

because H-mordenite increases the number of acidic sites on the exterior surface, changes the pore geometry, and improves the rate of diffusion to the catalyst surface. Yang *et al.* (7) studied the effect of the matrix on the Ni and V poisoning of USY zeolite and found that the presence of the matrix (e.g., SiO_2 and γ-Al_2O_3) can increase the resistance of USY to steam deactivation. In addition, toluene disproportionation by NiS/SiO_2 and USY zeolite (8) and xylene isomerization by NiS/γ-Al_2O_3 and USY zeolite (9, 10) were studied, and both NiS/SiO_2 and NiS/γ-Al_2O_3 significantly increase the activity of the USY zeolite, which is believed to relate to hydrogen spillover. More recently, Yumoto (11) reported a new type of γ-Al_2O_3–zeolite-based catalyst for deep HDS, and found that a small amount of zeolite accelerates the hydrogenation rate of the DBT ring.

In contrast, the HDS catalytic potential of zeolite addition to conventional Ni–Mo/γ-Al_2O_3 catalysts remains poorly understood. The distribution and local chemical environment of Ni and Mo and their relationship to catalytic activities of γ-Al_2O_3–USY zeolite-supported catalyst are not known. Optimization of Ni–Mo/γ-Al_2O_3–USY catalysts for various hydrotreating reactions also requires an understanding of the nature of the catalytic sites (i.e., on the types of acid sites present in the materials, the distribution of Ni and Mo between the alumina and zeolite, and the local chemical environment of the metals). Thus, in the present work, the HC reactions of DPM and the HDS of DBT were carried out to examine the activity of γ-Al_2O_3–USY zeolite-supported catalysts. The surface acidity of these catalysts was examined using NH_3 temperature-programmed desorption (TPD). The surface concentration of Ni and Mo species in both calcined and sulfided catalysts was determined by X-ray photoelectron spectroscopy (XPS). The distribution and local structural environment of Ni and Mo species in the bulk were studied by diffuse reflectance spectroscopy (DRS), high-resolution transmission electron microscopy (HRTEM), energy-dispersive spectroscopy (EDS), irradiated neutron activation analysis (INAA) and inductively coupled plasma emission spectroscopy (ICP-ES).

EXPERIMENTAL

Catalyst Preparation

The γ-Al_2O_3–zeolite support, provided by Catalysts & Chemical Industry Ltd., Japan, was prepared by extruding a mixture of ultrastable Y (USY) zeolite and γ-Al_2O_3 powder into pellets with a diameter of about 1 mm and calcining at 500°C for 1 h. The γ-Al_2O_3–zeolite support (designated as AZ) contains 60 wt% USY zeolite ($SiO_2/Al_2O_3 =$ 4.99, BET surface area = 756 m^2/g) and 40 wt% γ-Al_2O_3 (BET surface area = 209 m^2/g, pore volume = 0.81 ml/g). Three series of Ni, Mo, and Ni–Mo catalysts supported on γ-Al_2O_3–USY zeolite (designated as Ni/AZ, Mo/AZ, and Ni–Mo/AZ, respectively) were prepared by wet impregnation of the γ-Al_2O_3–USY zeolite extrudes (20 g) with aqueous solutions of $Ni(NO_3)_2 \cdot 6H_2O$, $(NH_4)_6Mo_7O_{24} \cdot 4H_2O$, and a mixture of both, respectively. The aqueous solutions were prepared by dissolving reagents to the desired concentrations in distilled water (9 ml) with additional aqueous ammonia (5 ml) at room temperature. In preparation of Ni–Mo catalysts, the total loading of Ni and Mo in the solutions was kept constant at 0.1236 mol per 100 g support (total zeolite + alumina). The pH values of the solutions were not measured in this work, but were probably about 8.0 based on our previous work using a similar protocol (12). After impregnation, the Ni/AZ, Mo/AZ, and Ni–Mo/AZ slurries were dried at 200°C for 2 h in a rotary kiln and then calcined at 550°C for 3 h in air. Thereafter, the catalysts were sulfided at 400°C for 2 h under a stream of H_2–H_2S (the volume percentage of H_2S in the mixture was 5.04%). In addition, a Ni–Mo/γ-Al_2O_3 catalyst was prepared following procedures identical to those above. γ-Al_2O_3 was the same as that used in γ-Al_2O_3–USY support. The nominal loadings of NiO and MoO_3 were 3 and 12 g, respectively, per 100 g γ-Al_2O_3 (total mole of NiO and MoO_3 was 0.1236 per 100 g γ-Al_2O_3, and that of NiO/MoO_3 was 0.48).

Catalytic Activity

DBT was dissolved in decalin to prepare a feedstock solution containing 1 wt% sulfur for the HDS of DBT. The HDS reaction of DBT and the HC reaction of diphenylmethane (DPM) were carried out using a batch microreactor at 340 and 375°C, respectively. Sulfided catalyst (0.3 g) and feedstock solution (10 ml) were loaded into the reactor. The reactor was tightly closed and filled with H_2 whose pressure in the reactor was set at 6.92 MPa. After 1 h reaction in a high-temperature furnace, the reactor was opened and the reactant solution was transferred into a vial for gas chromatography (GC) analysis. Hence, some gas-phase products were not detected and the selectivity was not calculated. For all catalytic reactions, the conversion rates were calculated based on the integrated areas of related target molecules in the GCs of the feedstock and the solution after reactions.

Catalyst Characterization

The bulk compositions of the catalysts were analyzed as follows: Ni and Mo were determined by INAA, and Si, Al, and Na were determined by ICP-ES. The distribution of Ni and Mo between zeolite and γ-Al_2O_3 was further examined by HRTEM and EDS analysis, with a spot size of about 30 nm. For TEM experiments, the fine powder samples of calcined Ni, Mo, and Ni–Mo catalysts supported on USY zeolite and γ-Al_2O_3 were deposited on carbon-coated TEM Cu grids. The specimens were studied using a JEOL 2010 high-resolution transmission electron microscope operated at 100 kV. The point-to-point resolution of the

microscope is 1.9 Å, and time duration for collecting EDS spectra was 100 s.

The NH_3 TPD measurements were carried out using a thermal analyzer DT-30 apparatus (Shimadzu, Japan). About 0.3 g of catalyst was heated in a glass tube under a He atmosphere at the rate of 30°C/min from room temperature to 500°C and kept at 500°C for an additional hour. After NH_3 adsorption at 150°C for 1 h, the sample was flushed with He for another hour and heated from 150 to 600°C at the rate of 10°C/min under the He atmosphere while the desorption of NH_3 was monitored.

X-Ray photoelectron spectra of the calcined and sulfided catalysts were collected at a chamber pressure of $\sim 10^{-9}$ Torr (1 Torr $= 1.33 \times 10^{-4}$ MPa) using a Phi-5500 ESCA spectrometer (Perkin–Elmer) and monochromatized Al$K\alpha$ ($h\nu = 1486.7$ eV) X rays. The X-ray photoelectron spectra were calibrated based on a C 1*s* binding energy of 284.6 eV. The Mo 3*d* and Ni 2*p* lines were decomposed by fitting. The decomposition of the Mo 3*d* envelope was based on several constraints to give physical significance to the peaks obtained: (1) the spin–orbit splitting of the Mo 3*d* peak is 3.15 eV; (2) the Mo $3d_{5/2}$/Mo $3d_{3/2}$ area ratio was kept constant at the theoretical value of 1.5; (3) the full widths at half-maximum (FWHMs) of the Mo $3d_{5/2}$ and Mo $3d_{3/2}$ peaks of the Mo^{5+} and Mo^{6+} oxidation states were kept equal to those of the Mo^{4+} species (13). The atomic concentration ratio on the surface of catalysts was calculated using $n_A/n_B = I_A S_B / I_B S_A$, where n_i is the atomic number of species i ($i =$ A or B), I_i is the integrated intensity of species i, and S_i is the sensitivity factor determined by XPS measurement (12). The sensitivity factor depends mainly on the photoionization cross section σ_i but also on exciting X-ray energy, takeoff angle, detector efficiency, and kinetic energy of the measured peaks. The formula used to calculate the atomic concentration was similar to the Kerkhof–Moulijn model (14).

The diffuse reflectance spectra of calcined Ni, Mo, and Ni–Mo catalysts supported on USY zeolite and γ-Al_2O_3 were measured using a Lambda-19 UV–Vis–NIR spectrometer (Perkin–Elmer) equipped with a lab sphere diffuse reflectance integrating attachment. The spectra were recorded over the range 200–2500 nm at room temperature with a slit of 4 mm. A quartz window was used in the DRS measurements, and its spectrum was subtracted from the spectra of the catalysts.

RESULTS

Catalytic Activity

The chemical compositions of Ni/γ-Al_2O_3–zeolite (Ni/AZ), Mo/γ-Al_2O_3–zeolite (Mo/AZ), and Ni–Mo/γ-Al_2O_3–zeolite (Ni-Mo/AZ) catalysts are shown in Table 1. The catalytic activities of sulfided Ni/AZ, Mo/AZ, and Ni–Mo/AZ catalysts for the HC of DPM and the HDS of DBT, as well as NiO content (mol%), MoO_3 content (mol%), and NiO/(NiO + MoO_3) ratio, are summarized in Table 2. For Ni/AZ, HC activity for DPM and HDS activity for DBT increased with NiO content to about 5 mol%, and then decreased with further increase of NiO, but this trend was less significant for the HC activity of DPM. For Mo/AZ, HC activity for DPM increased with MoO_3 content, and HDS activity for DBT increased up to about 5 mol% MoO_3 and then decreased slightly with MoO_3 content. For Ni–Mo/AZ, HC activity for DPM generally decreased with increase in NiO/(NiO + MoO_3) ratio; however, HDS activity of DBT reached a prominent maximum at a NiO/(NiO + MoO_3) ratio of about 0.4. In comparison, the HDS activity for DBT and HC activity for DPM over a Ni–Mo/γ-Al_2O_3 catalyst was included in Table 2. The HC activity for DPM remained very similar for the three series of Ni/AZ, Mo/AZ, and Ni–Mo/AZ catalysts, but was significantly higher than that of the Ni–Mo/γ-Al_2O_3 catalyst. HDS activity for DBT over Ni–Mo/AZ catalysts was slightly improved compared with that for conventional Ni–Mo/γ-Al_2O_3 catalysts.

TABLE 1

Chemical Composition (wt%) of Ni and Mo Catalysts Supported on γ-Al_2O_3–USY Zeolite[a]

Sample	SiO_2	Al_2O_3	Na_2O	NiO	MoO_3
Ni/γ-Al_2O_3–zeolite					
Ni/AZ-1	42.76	38.87	0.13	1.43	0.01
Ni/AZ-2	42.36	38.23	0.11	2.95	0.01
Ni/AZ-3	41.75	37.70	0.11	4.19	0.02
Ni/AZ-4	39.64	36.51	0.08	5.41	0.01
Ni/AZ-5[b]	39.63	35.75	0.09	6.86	0.02
Mo/γ-Al_2O_3–zeolite					
Mo/AZ-1	39.60	35.72	0.10	<0.01	2.78
Mo/AZ-2	39.68	35.66	0.09	<0.01	5.81
Mo/AZ-3	39.60	36.09	0.08	<0.01	7.94
Mo/AZ-4	36.29	33.32	0.11	<0.01	9.90
Mo/AZ-5[b]	35.87	32.34	0.09	<0.01	12.33
Ni–Mo/γ-Al_2O_3–zeolite					
Ni–Mo/AZ-1	35.87	32.34	0.09	<0.01	12.33
Ni–Mo/AZ-2	37.17	34.01	0.06	1.40	9.66
Ni–Mo/AZ-3	37.21	33.59	0.08	1.91	8.57
Ni–Mo/AZ-4	37.66	33.92	0.08	2.62	7.65
Ni–Mo/AZ-5	37.74	33.93	0.09	3.31	6.45
Ni–Mo/AZ-6	38.00	34.17	0.09	3.92	5.27
Ni–Mo/AZ-7	38.17	34.35	0.10	5.04	2.64
Ni–Mo/AZ-8	39.63	35.75	0.09	6.86	0.02

[a] The contents of SiO_2, Al_2O_3, and Na_2O were determined by ICP-ES, and the contents of NiO and MoO_3 by INAA.

[b] Samples Ni/AZ-5 and Ni–Mo/AZ-8 are the same; samples Mo/AZ-5 and Ni–Mo/AZ-1 are the same.

Surface Acidity

The NH_3 TPD profiles of calcined and sulfided Ni/AZ, Mo/AZ, and Ni-Mo/AZ catalysts were similar to that of

TABLE 2

Metal Contents, Catalytic Activity, and Acidity of Ni, Mo, and Ni–Mo Sulfide Catalysts Supported on γ-Al_2O_3–USY Zeolite

	Metal content (mol%)	Activity (%)		Acidity (mmol/g)			
				Calcined		Sulfided	
		HDS (DBT)	HC (DPM)	Site I	Site II	Site I	Site II
Ni catalysts	NiO						
Ni/AZ-1	1.75	65.9	21.7	0.52	0.31	0.50	0.32
Ni/AZ-2	3.52	80.5	31.4				
Ni/AZ-3	5.00	83.7	32.9	0.61	0.35	0.66	0.37
Ni/AZ-4	6.64	81.5	31.6				
Ni/AZ-5[a]	8.33	72.9	30.8	0.41	0.37	0.48	0.32
Mo catalysts	MoO_3						
Mo/AZ-1	1.87	53.6	25.8	0.36	0.28	0.40	0.34
Mo/AZ-2	3.84	59.9	29.1				
Mo/AZ-3	5.15	59.6	31.8	0.61	0.42	0.44	0.41
Mo/AZ-4	6.87	57.4	35.0				
Mo/AZ-5[a]	8.55	55.1	46.2	0.74	0.53	0.46	0.34
Ni–Mo catalysts	Ni/(Ni + Mo)						
Ni–Mo/AZ-1	<0.0016	55.1	46.2	0.74	0.53	0.46	0.34
Ni–Mo/AZ-2	0.2184	73.2	40.9				
Ni–Mo/AZ-3	0.3005	93.4	38.4				
Ni–Mo/AZ-4	0.3977	99.5	37.7	0.74	0.40	0.69	0.51
Ni–Mo/AZ-5	0.4974	87.2	39.9				
Ni–Mo/AZ-6	0.5892	84.7	39.9				
Ni–Mo/AZ-7	0.7864	81.1	35.8	0.66	0.33	0.78	0.45
Ni–Mo/AZ-8	0.9985	72.9	35.8	0.41	0.37	0.48	0.32
γ-Al_2O_3–USY				0.39	0.27		
Ni–Mo/γ-Al_2O_3	0.3253	87.5	5.4	0.24	0.14	0.28	0.17

[a] Samples Ni/AZ-5 and Ni–Mo/AZ-8 are the same; and samples Mo/AZ-5 and Ni–Mo/AZ-1 are the same.

γ-Al_2O_3–USY zeolite support and also similar to those of alumina-supported Ni–Mo catalysts (15). Two major acid sites were observed. The dominant desorption peak (acid site I) occurred at about 250°C, which corresponds to a Lewis-type acid site (16). An additional desorption peak (acid site II) occurred at about 400°C, which corresponds to a Brønsted-type acid site (16). The sulfidation did not change the acidic structures dramatically. NH_3 TPD profiles were decomposed by fitting, and the integrated areas of the two major acid sites represented their acid densities (Table 2). For Ni/AZ, the acid densities of the two sites of both calcined and sulfided catalysts increased with an increase in NiO content up to about 5 mol%, and then tended to decrease. For Mo/AZ, the content of MoO_3 tended to increase the acid densities of the two acid sites for both calcined and sulfided catalysts. For calcined Ni–Mo/AZ catalysts, the acid densities of the two acid sites decreased slightly with increase in $NiO/(NiO + MoO_3)$ ratio. After sulfidation, the acid densities of the two acid sites tended to increase and then decrease slightly with increase in $NiO/(NiO + MoO_3)$ ratio. The densities of the acid sites in Ni, Mo, and Ni–Mo catalysts supported on γ-Al_2O_3–USY zeolite were higher than those in the Ni–Mo/γ-Al_2O_3 catalyst, as well as in the γ-Al_2O_3–USY zeolite support.

Surface Concentration of Ni and Mo Species

X-Ray photoelectron spectra of calcined and sulfided Ni/AZ, Mo/AZ, and Ni–Mo/AZ catalysts were similar to those of Ni–Mo/γ-Al_2O_3–B_2O_3 in profile (12). The two prominent peaks were assigned to the spin-splitting Mo^{6+} $3d_{5/2}$ (BE ≅ 232.6 eV, where BE is binding energy) and Mo^{6+} $3d_{3/2}$ (BE ≅ 235.8 eV) lines of Mo oxide species. The Mo 3*d* X-ray photoelectron spectra of the sulfided catalysts were decomposed into three sets of doublets, corresponding to Mo^{6+}, Mo^{5+}, and Mo^{4+} species in order of decreasing binding energy, and a broad peak at about 226.3 eV assigned to S 2*s*. The Mo^{6+} species may be MoO_3 or another oxide phase that is not completely sulfided, the Mo^{5+} species may be a Mo oxysulfide species, and the Mo^{4+} species are MoS_2 and the Ni–Mo–S phase under the sulfidation conditions (1). The two main peaks in the Ni 2*p* X-ray photoelectron spectra of calcined samples were assigned to the spin-splitting Ni $2p_{3/2}$ (BE ≅ 856.3 eV) and Ni $2p_{1/2}$ (BE ≅ 873.8 eV) and

the two broad peaks to the envelopes of the corresponding satellite lines. The Ni 2*p* XPS spectra of the sulfided catalysts were more complex and were decomposed into two sets of Gaussian components (one for the Ni oxide species, as seen in the calcined catalysts, and the other for the Ni sulfide species). The Ni sulfide species were assumed to be Ni_3S_2 and the so-called Ni–Mo–S phase under the sulfidation conditions (1), which were responsible for the active catalysis.

The atomic concentrations of Ni and Mo species on the surface of calcined and sulfided Ni/AZ, Mo/AZ, and Ni–Mo/AZ catalysts were calculated following the procedure of Li *et al.* (12). Figure 1 shows variations of Ni/Al and Mo/Al atomic ratios on the surface of calcined and sulfided Ni/AZ and Mo/AZ catalysts as functions of the contents of NiO and MoO_3 in the bulk. The Ni/Al ratio reached a maximum at an NiO content of about 5 mol% for both calcined and sulfided Ni catalysts. The Ni/Al ratio on the surface was dramatically higher than that in the bulk. For Mo/AZ, the Mo/Al ratio increased with the bulk content of MoO_3 for both calcined and sulfided Mo catalysts. Mo/Al ratios on the surface and in the bulk of calcined Mo/AZ catalysts were not significantly different, although the Mo/Al ratio on the surface was slightly lower than that for the bulk at the highest content of MoO_3.

Figure 2 shows variations of Ni/Al and Mo/Al atomic ratios with the bulk $NiO/(NiO + MoO_3)$ ratio for calcined and sulfided Ni–Mo/AZ catalysts. The Ni/Al atomic ratio reached a maximum at $NiO/(NiO + MoO_3)$ ratios of 0.5 and 0.6, respectively, for calcined and sulfided catalysts. The

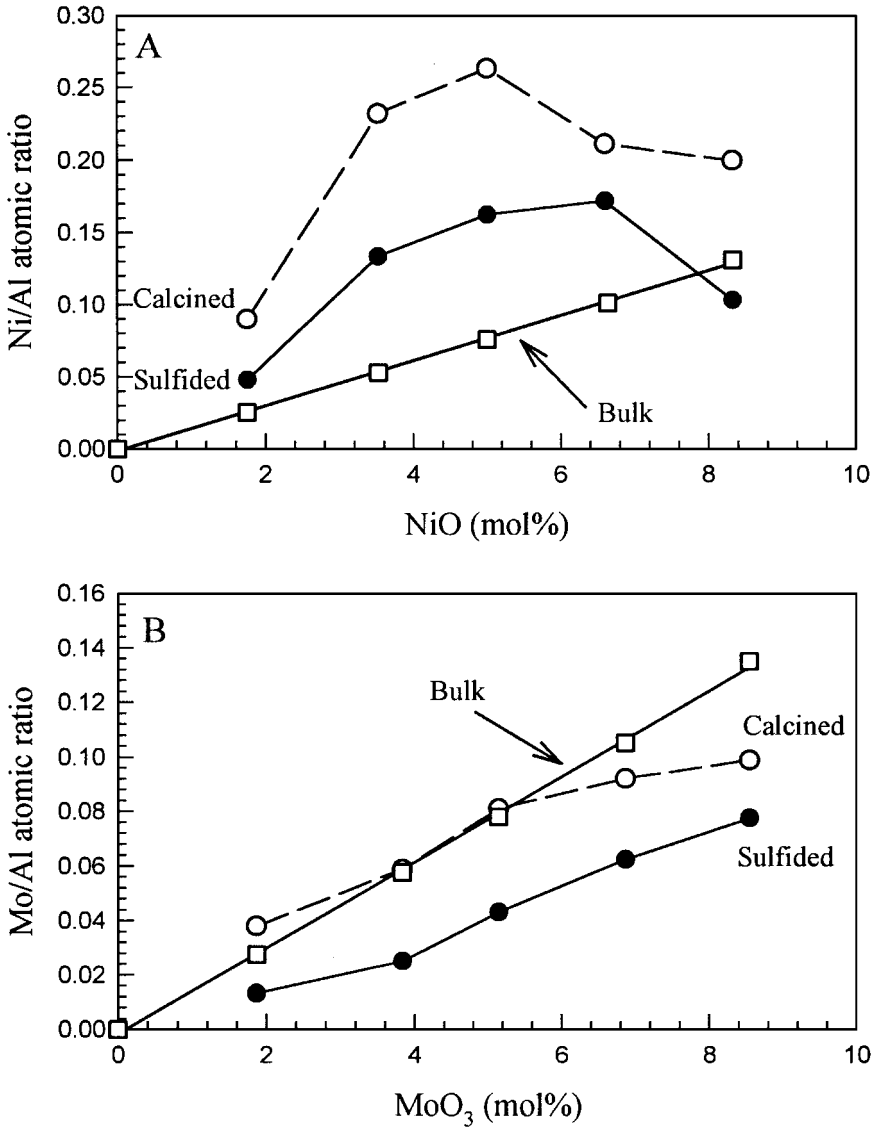

FIG. 1. Ni/Al and Mo/Al atomic ratios on the surface as functions of the bulk content (mol%) of NiO in Ni/γ-Al_2O_3–USY zeolite (A) and MoO_3 in Mo/γ-Al_2O_3–USY zeolite (B), respectively. The surface atomic concentrations were calculated by XPS measurements.

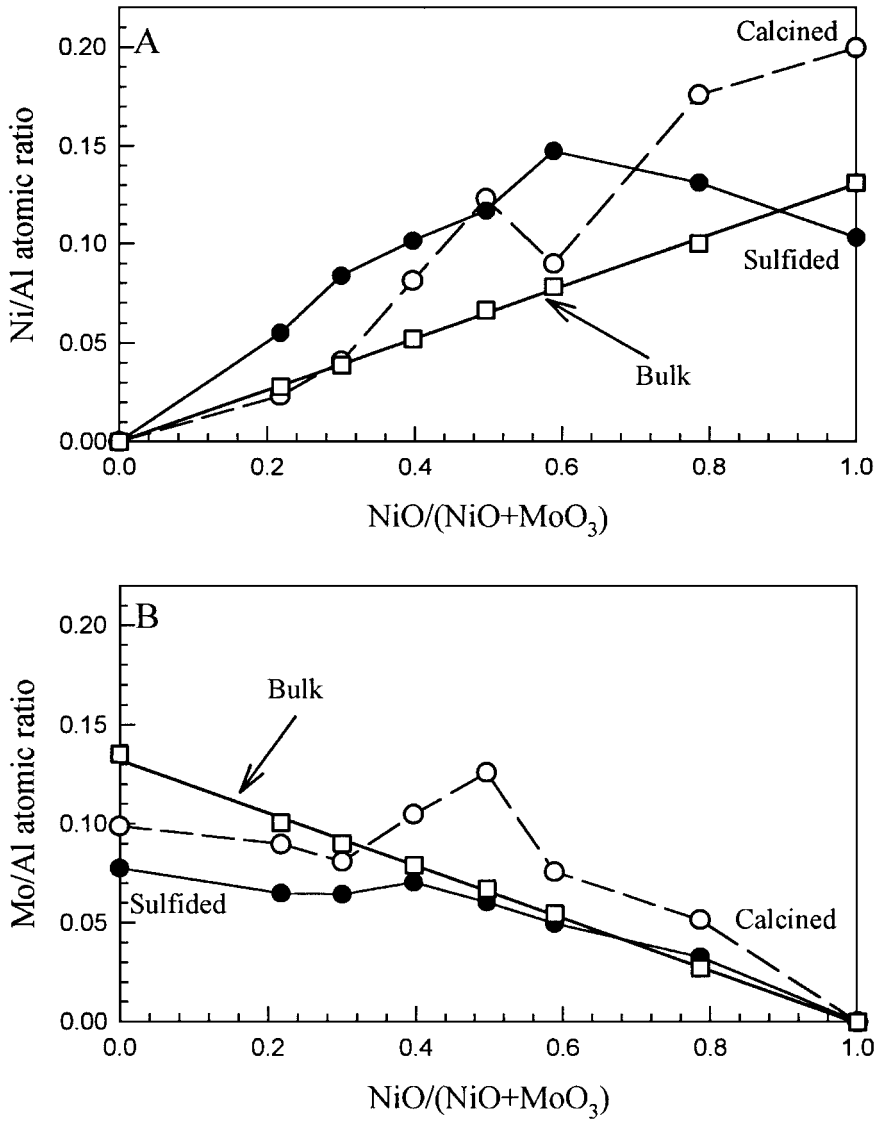

FIG. 2. Ni/Al (A) and Mo/Al (B) atomic ratios on the surface of Ni–Mo/γ-Al_2O_3–USY zeolite as a function of the NiO/(NiO + MoO_3) ratio. The surface atomic concentrations were calculated by XPS measurements.

sulfidation significantly changed the distribution of Ni on the surface: where the NiO content was low, the concentration of Ni species on the surface was increased relative to the bulk or the calcined sample; but where the NiO content was high, the NiO species on the surface were not fully sulfided. The Mo/Al atomic ratio showed a maximum at bulk NiO/(NiO + MoO_3) ratios of 0.5 and 0.4, respectively, for calcined and sulfided catalysts.

The extent of sulfidation of Ni and Mo species was calculated based on the atomic concentration ratios of the corresponding sulfide species over the total oxide and sulfide species. The extent of sulfidation of Mo species reached a maximum at a MoO_3 content of about 5 mol% (Fig. 3A). However, the sulfidation of Ni species essentially remained unchanged, although there is a slight maximum at a NiO content of about 5 mol% (Fig. 3A). The extent of sulfidation of both Ni and Mo species in Ni–Mo/AZ catalysts showed a maximum at a NiO/(NiO + MoO_3) ratio of about 0.2–0.5 (Fig. 3B).

Figure 4 shows the correlation between the Ni/(Ni + Mo) atomic ratio on the surface (as determined by XPS) and the NiO/(NiO + MoO_3) ratio in the bulk (as determined by INAA) for both calcined and sulfided Ni–Mo/AZ catalysts. This correlation was essentially linear with a slope of 1 for the calcined catalysts, indicating that both Ni and Mo species were distributed uniformly in the bulk and on the surface of the calcined catalysts. However, this correlation was nonlinear for sulfided catalysts, indicating that the sulfidation caused redistribution of Ni and/or Mo species and enrichment of the Ni species on the surface.

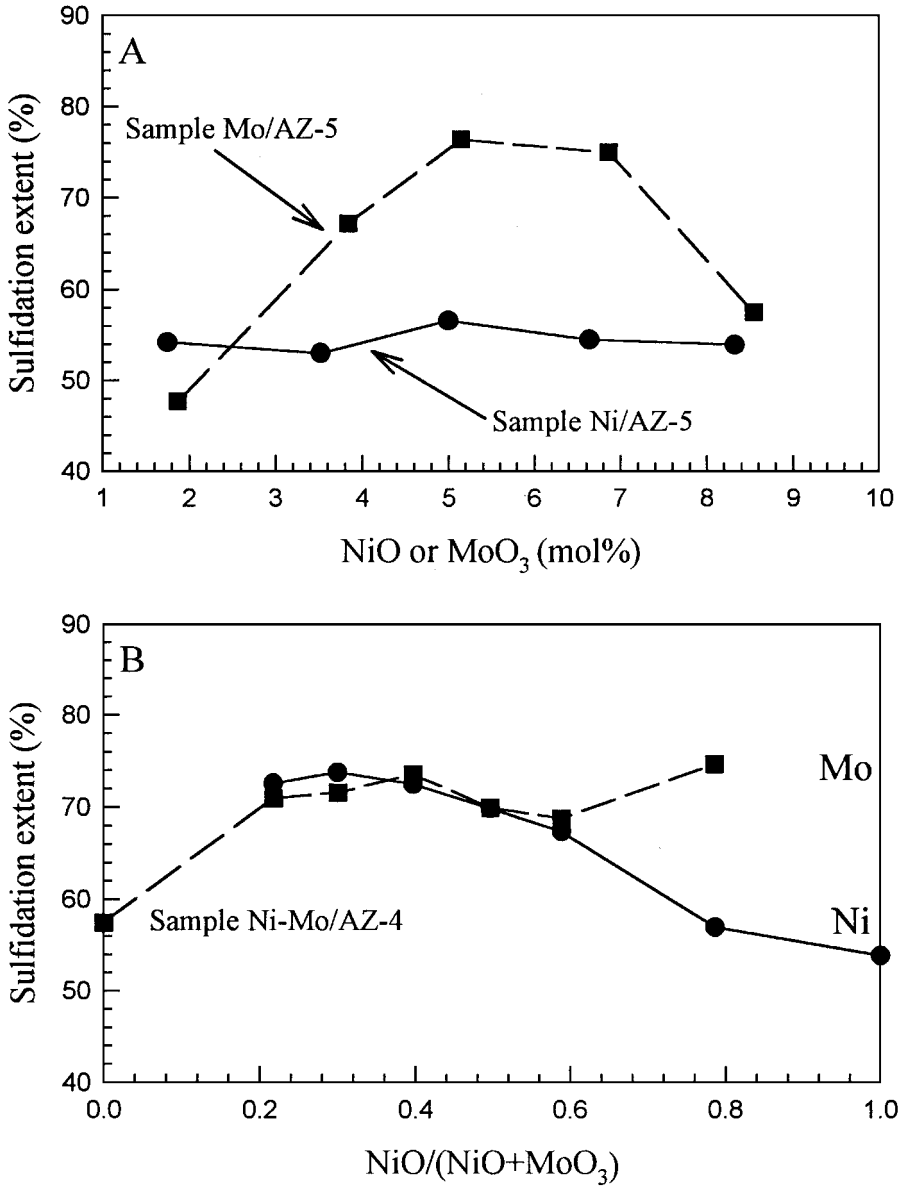

FIG. 3. Sulfidation extent (%) of Ni (filled circles and solid lines) and Mo (filled squares and dashed lines) species in Ni/γ-Al_2O_3–USY zeolite and Mo/γ-Al_2O_3–USY zeolite (A) and in Ni–Mo/γ-Al_2O_3–USY zeolite (B) catalysts, as a function of their bulk compositions. The sulfidation extent was calculated based on the integrated area ratio of sulfided species over the total Ni or Mo species measured by XPS.

Distribution and Structure of Ni and Mo Species in the Bulk

Figure 5 shows TEM images of a representative Ni–Mo/AZ catalyst (Ni–Mo/AZ-4). Zeolite particles were surrounded by γ-Al_2O_3 that appears as more transparent aggregates (Fig. 5A). The zeolite was crystalline, as indicated by its selected area electron diffraction (SAED) pattern (Fig. 5B). Both Ni and Mo were detected by EDS of the zeolite particles (Fig. 5C). γ-Al_2O_3 was also crystalline, although the high-magnification image did not show any fringes (Fig. 5D). However, the SAED pattern showed two rings (Fig. 5E), indicating that γ-Al_2O_3 was a very fine powder, in good agreement with the powder XRD pattern of γ-Al_2O_3 showing broad diffraction peaks (15). Both Ni and Mo were associated with alumina particles, but the concentration of Mo in alumina was dramatically higher than it was in zeolite particles (Fig. 5F). No Ni and Mo aggregates were observed in this catalyst sample. However, the high-magnification TEM image of another Ni/AZ catalyst with high content of NiO (Ni/AZ-5) shows several nanometer-size particles in γ-Al_2O_3 (Fig. 6A). The EDS spectrum indicated that these particles were Ni oxides (Fig. 6B). Al and Si were detected in the EDS spectrum, because the Ni

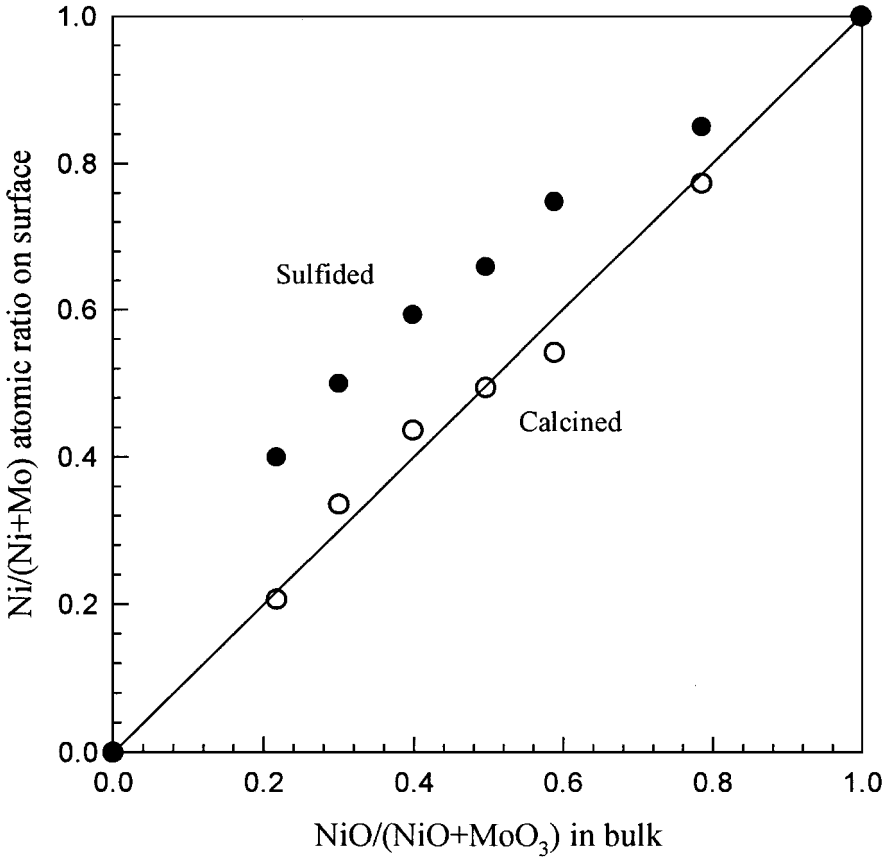

FIG. 4. Variation of surface Ni/(Ni + Mo) atomic ratio in calcined (open circles) and sulfided (filled circles) Ni–Mo/γ-Al_2O_3–USY zeolite catalysts with the bulk NiO/(NiO + MoO_3) ratio. The solid line is 1 : 1 for comparison. Atomic concentrations of Ni and Mo on the surface were determined by XPS; the contents of Ni and Mo in the bulk were determined by INAA (Table 1).

oxide particles were smaller than the spot size of the electron beam. One of these Ni oxide particles was examined (inset to Fig. 6A), and the *d* space measured on the basis of the fringes was about 2.0 Å, in good agreement with the d_{012} space (2.088 Å) of NiO (JCPDS 44-1159). Thus, the Ni oxide particles were NiO.

To determine the distribution of Ni and Mo between zeolite and γ-Al_2O_3, the chemical compositions (Si, Al, Ni, and Mo) of Ni/AZ-5, Mo/AZ-5, and Ni-Mo/AZ-4 catalysts were semiquantitatively determined by EDS analysis using a spot size of ~30 nm. The contents (wt%) of NiO and/or MoO_3 for different spots analyzed were plotted against weight percentage Al_2O_3 (Fig. 7). For the pure Ni catalyst, the content of NiO remained essentially unchanged over the range of weight percentage Al_2O_3, indicating that the contents of NiO in zeolite and γ-Al_2O_3 were very similar and close to its bulk content (Table 1). For the pure Mo catalysts, the content of MoO_3 increased significantly with weight percentage Al_2O_3, indicating that Mo may be preferentially associated with γ-Al_2O_3. Similarly, for the Ni–Mo catalyst, the weight percentage NiO was unrelated to the total weight percentage Al_2O_3, but the weight percentage MoO_3 increased with weight percentage Al_2O_3. Thus, Ni was essentially uniformly distributed in all the catalysts, and its content on a microscopic scale was close to its bulk composition. However, Mo was clearly associated with γ-Al_2O_3.

Figure 8 shows the diffuse reflectance spectra of calcined Ni/AZ, Mo/AZ, and Ni–Mo/AZ catalysts. The diffuse reflectance spectra of Ni catalysts were complex (Fig. 8A): there were three broad absorption bands between 380 and 1300 nm, located at about 410, 722, and 1150 nm. The three main absorption bands were assigned to the three allowed transitions characteristic of six-coordinated Ni^{2+} (17–19). In addition, there were two other peaks at about 250 and 295 nm, which may be due to Ni^{2+}–O charge transfer transitions. It is unclear why the intensity of the peaks at 250 and 395 nm was so high for Ni/AZ-5 catalyst (NiO = 8.33 mol%). However, the visible diffuse reflectance spectrum of the Ni/AZ-5 catalyst was similar to that of NiO, indicating that NiO aggregates formed, as characterized by the sharp peak at about 395 nm (20). Ni may be incorporated into the surface vacancies of γ-Al_2O_3 and zeolite in the other two catalysts with lower content of NiO.

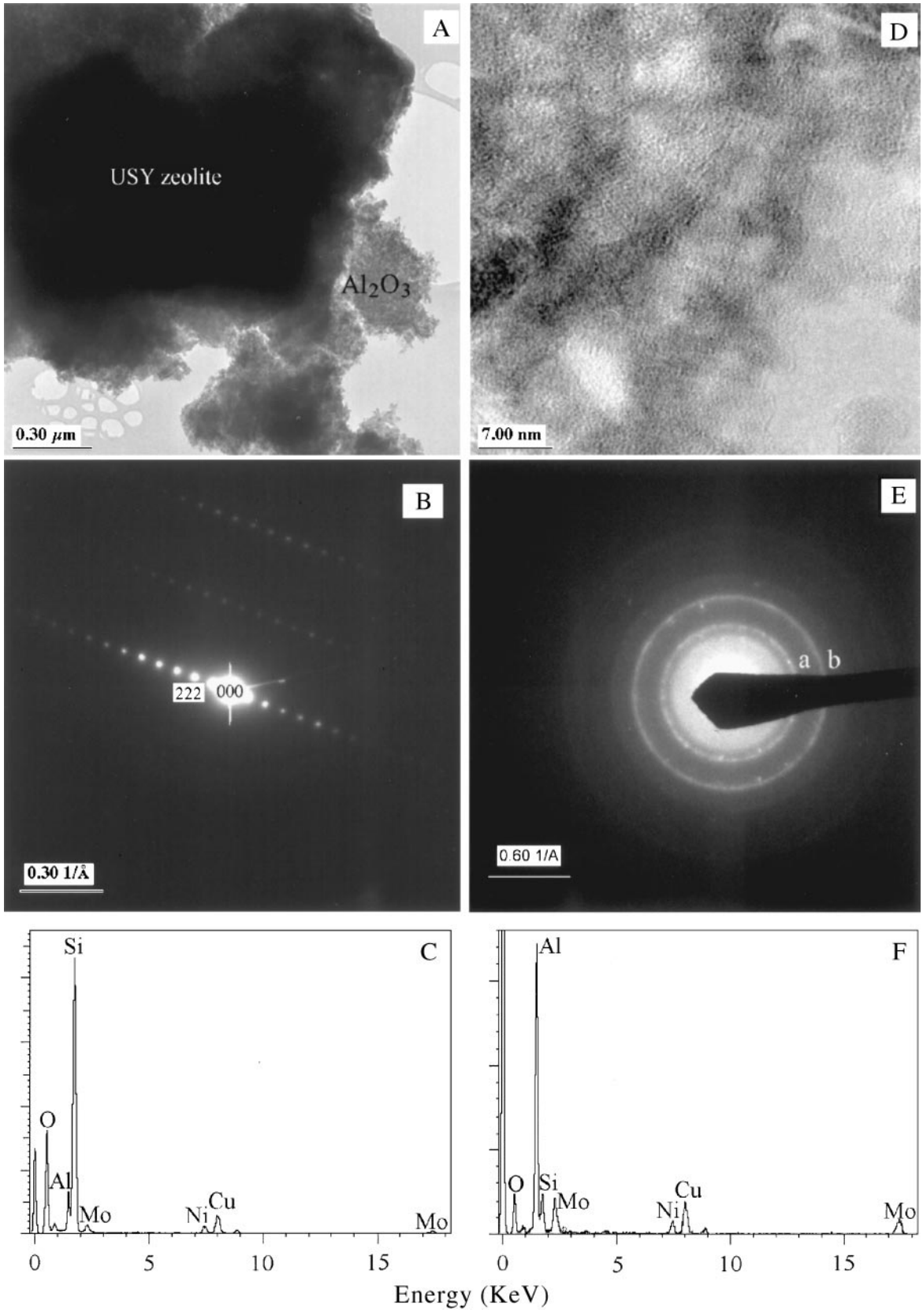

FIG. 5. TEM images of a Ni–Mo/γ-Al_2O_3–zeolite (sample Ni–Mo/AZ-4) catalyst. (A) Low-magnification images showing both zeolite and γ-Al_2O_3. (B) Selected area electron diffraction (SAED) pattern of zeolite. (C) Energy-dispersive X-ray (EDS) spectrum collected on zeolite particle. (D) High-magnification image of γ-Al_2O_3. (E) SAED pattern of γ-Al_2O_3: (a) $d = 2.01$ Å, (b) $d = 1.42$ Å. (F) EDS spectrum collected on γ-Al_2O_3 particle.

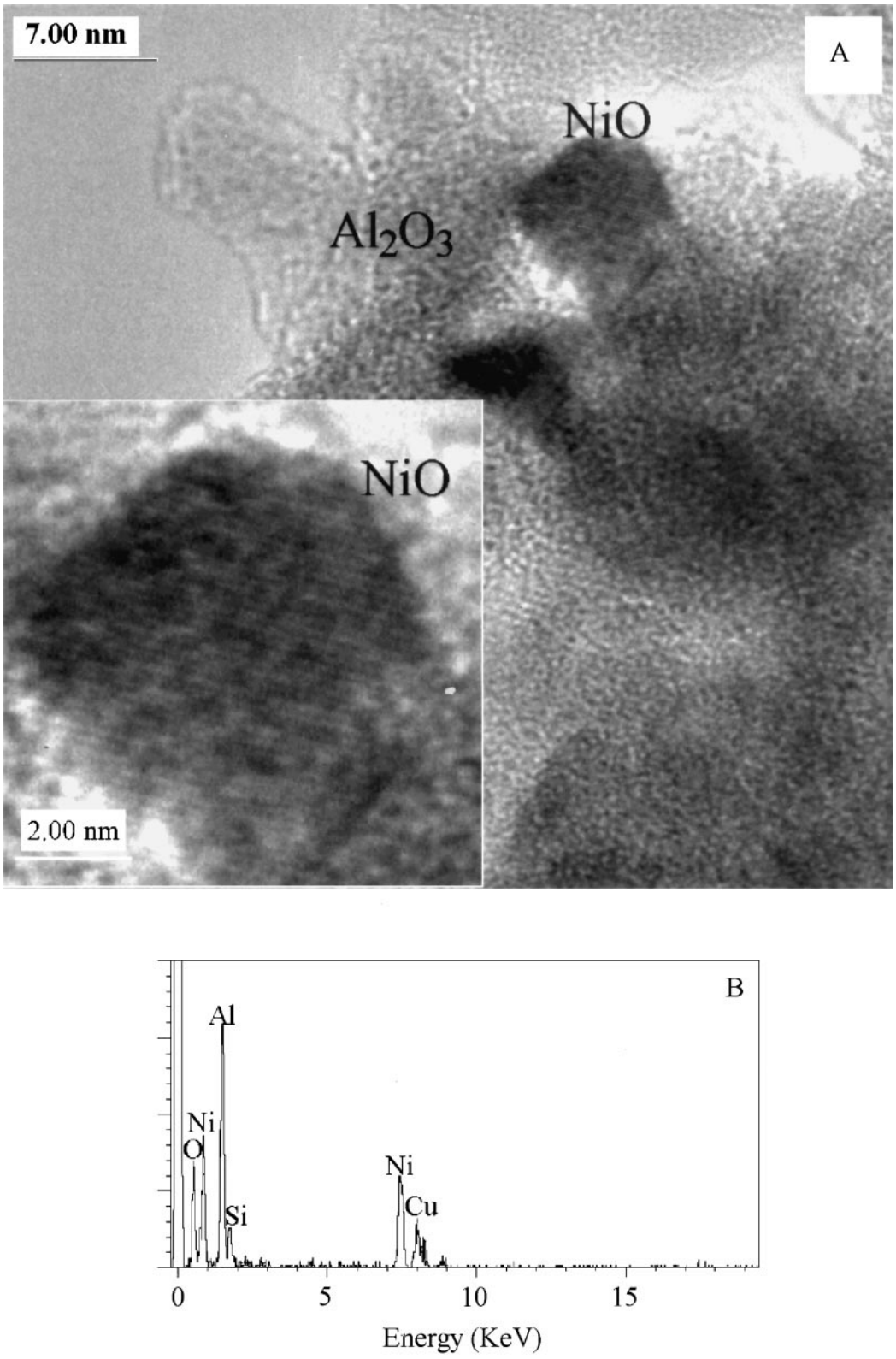

FIG. 6. High-magnification TEM (A) image and EDS spectrum (B) of a Ni/γ-Al_2O_3–USY zeolite catalyst (Ni/AZ-5) in which the NiO content is 8.33 mol%. Lattice fringes of one NiO particle well shown in the inset were measured.

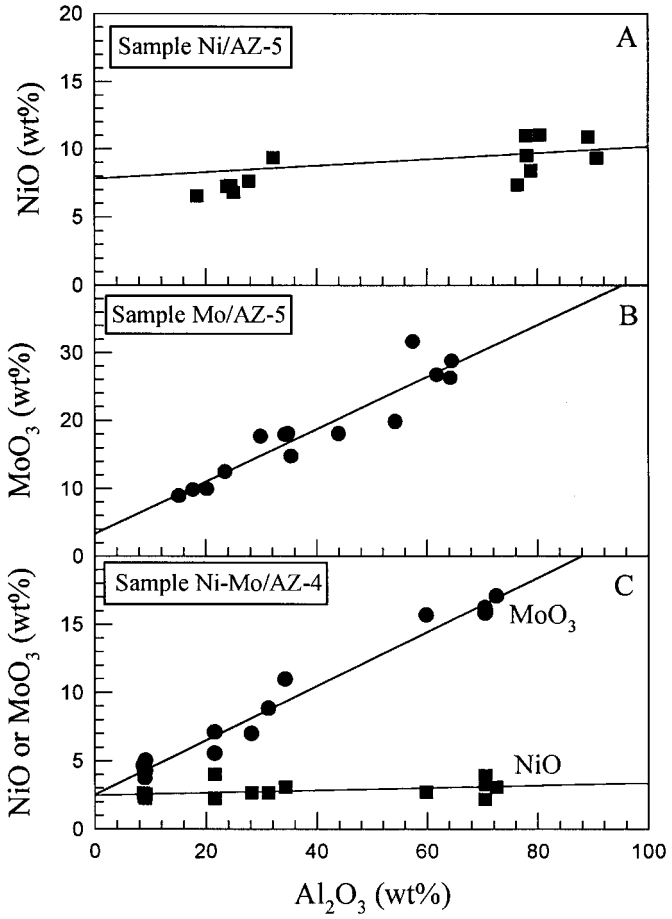

FIG. 7. Variation of weight percentage NiO and/or MoO_3 as a function of total weight percentage Al_2O_3 (in zeolite and/or alumina) for TEM analyses (~30 nm in spot size) of Ni/AZ-5 (A), Mo/AZ-5 (B), and Ni–Mo/AZ-4 (C).

The diffuse reflectance spectra suggest the presence of Ni in tetrahedral or trigonal coordination, but this was not conclusive by comparison with spectra reported in the literature (21, 22).

Figure 8B shows the DRS spectra of calcined Mo catalysts in the range 200–1300 nm, compared with the DRS spectrum of MoO_3. The broad peak between 200 and 500 nm (shown in the inset) was decomposed into three Gaussian components by fitting (23) and assigned to Mo^{6+}–O charge transfer transitions. The peak at about 250 nm was attributed to tetrahedrally coordinated Mo^{6+}, and the peaks at about 290 and 350 nm to octahedrally coordinated Mo^{6+} (24, 25). Thus, both four-coordinate ($^{[4]}Mo^{6+}$) and six-coordinated ($^{[6]}Mo^{6+}$) species were present in the calcined Mo/γ-Al_2O_3–zeolite catalysts. The ratio $^{[4]}Mo^{6+}/^{[6]}Mo^{6+}$ tended to decrease with increasing MoO_3 content, but a more quantitative determination of this ratio may be difficult because the peak at about 250 nm may also have a contribution from $^{[6]}Mo^{6+}$. In Fig. 8C, the absorption edge peaks due to Ni^{2+}–O and Mo^{6+}–O charge-transfer transitions overlapped. In this case the information DRS provided on the structure of Ni and Mo was limited.

DISCUSSION

Interaction of Aqueous Ni and Mo Species with the Surface of Supports

The pH values of aqueous $Ni(NO_3)_2 \cdot 6H_2O$, $(NH_4)_6Mo_7O_{24} \cdot 4H_2O$, and their coaqueous solutions were not measured in this work, but the pH value of the coaqueous Ni–Mo solutions was probably close to 8 based on our previous work (12). At this pH value, γ-Al_2O_3 has a slightly negative-charged external surface, and USY zeolite has a negatively charged external surface and internal framework (26, 27). In addition, at this pH, Ni^{2+} should be the dominant Ni species (27, 28) and MoO_4^{2-} should be the dominant Mo species (26, 28, 29). Based on charge, Ni should have a strong electrostatic attractive interaction with the external surface of γ-Al_2O_3 and USY zeolite and with the internal framework of USY zeolite (i.e., it would be cation exchanged). However, the electrostatic interaction of MoO_4^{2-} with the external surface of γ-Al_2O_3 and USY zeolite or the internal framework of USY zeolite should be repulsive (i.e., it would not cation exchange into USY zeolite). However, MoO_4^{2-} may form inner sphere complexes with the external surface of γ-Al_2O_3 (29–31). Hence, one would predict that, during the ion-exchange stage, Ni^{2+} would be associated with both materials, but MoO_4^{2-} would be preferentially associated with the external surface of γ-Al_2O_3 which has a less negative surface charge. During calcination, both Ni and Mo speices may have been redistributed between γ-Al_2O_3 and the USY zeolite. Consequently, one would predict that following calcination, Ni would be distributed in vacancies on the surface of γ-Al_2O_3 and USY zeolite or in the supercavity and sodalite cage of USY zeolite, or would even form nickel oxide aggregates at a higher NiO loading (e.g., >5 mol%). In contrast, Mo would be dominantly distributed in vacancies on the surface of γ-Al_2O_3, but also in the surface vacancies or internal pores of USY zeolite (due to redistribution during calcination). Indeed, these redistributions of Mo and Ni are broadly consistent with our observations.

Nature and Distribution of Metals versus Catalytic Activity

Ni/AZ catalysts. In Ni/AZ catalysts, the contents of NiO in γ-Al_2O_3 and zeolite were similar and close to the average content of the bulk sample (Fig. 7A, Table 1). Thus, the distribution of Ni between γ-Al_2O_3 and zeolite was not significantly different. However, XPS analysis indicated that the Ni/Al atomic ratio on the surface reached a maximum at a NiO content of about 5 mol%, and decreased with further increase in NiO content (Fig. 1A). These results suggested

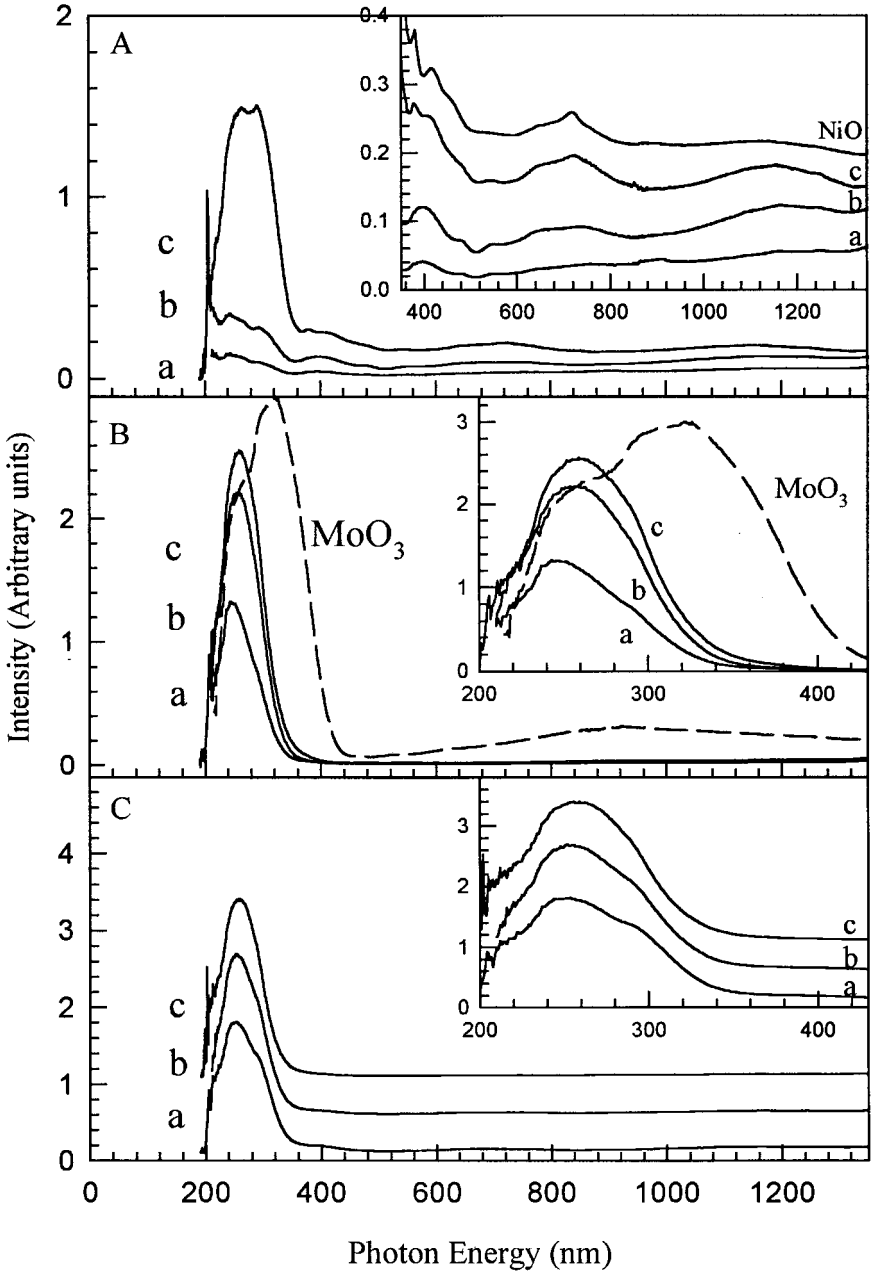

FIG. 8. Diffuse reflectance spectra of Ni/γ-Al_2O_3–USY zeolite (A), Mo/γ-Al_2O_3–USY zeolite (B), and Ni–Mo/γ-Al_2O_3–USY zeolite (C). The chemical compositions of these catalysts are given in Table 1. (A) (a) Ni/AZ-1, (b) Ni/AZ-3, (c) Ni/AZ-5. (B) (a) Mo/AZ-1, (b) Mo/AZ-3, (c) Mo/AZ-5. (C) (a) Ni–Mo/AZ-6, (b) Ni–Mo/AZ-4, (c) Ni–Mo/AZ-2.

that the Ni species formed monolayers on the surface of γ-Al_2O_3 and USY zeolite particles or became incorporated into the supercavity and sodalite cage of USY zeolite when the NiO content was below 5 mol%. However, the extra Ni may have formed Ni oxide aggregates with a further increase in NiO, and the dispersion of Ni species was reduced, in good agreement with the diffuse reflectance spectra and TEM observations. The visible diffuse reflectance spectrum of a Ni/γ-Al_2O_3–USY zeolite (Ni/AZ-5) containing 8.33 mol% NiO was very similar to that of NiO, but different from the diffuse reflectance spectra of the other two Ni catalysts (Fig. 8A). In addition, a high-magnification TEM image also showed the presence of NiO in the Ni/AZ-5 catalyst (Fig. 6). Regardless of the interpretation chosen for the distribution of Ni, it is clear that Ni was dominantly six-coordinated. A very small amount of Ni may have been in tetrahedral or trigonal coordination. The HDS activity of Ni/AZ catalysts was related to the content, dispersion, and

sulfidation of Ni species. The Ni species was well dispersed and better sulfided at a NiO content of about 5 mol% (Figs. 1A, 3A), but NiO aggregates formed and the dispersion of Ni species decreased with increasing content of NiO. Thus, the HDS activity for DBT over Ni/γ-Al_2O_3–USY zeolite catalysts increased up to 5 mol% NiO and then decreased with increasing NiO content.

Mo/AZ catalysts. In Mo/AZ catalysts, Mo was preferentially associated with γ-Al_2O_3 (Fig. 7B), forming either monolayers or Mo oxide aggregates. The MoO_3 concentration on the surface was generally close to that in the bulk samples, and deviated from the bulk composition slightly at higher MoO_3 content (Fig. 1B, Table 1), indicating that the dispersion of Mo species decreased. Thus, when the MoO_3 content was below about 5 mol%, Mo species were distributed as monolayers on the surface of γ-Al_2O_3 particles mainly, but also on the surface of USY zeolite particles. With an increase in MoO_3 content, Mo oxide aggregates may have appeared, which resulted in a decrease in its dispersion and extent of sulfidation (Fig. 3A). The diffuse reflectance spectra show that Mo may be tetrahedrally or octahedrally coordinated: when MoO_3 content was low, Mo was mainly tetrahedrally coordinated, but the proportion of octahedrally coordinated Mo species increased with MoO_3 content (25). The HDS of DBT over Mo/AZ catalysts was also high, and showed a marginal maximum at a MoO_3 content of about 5 mol%, which is attributed mainly to the higher dispersion and sulfidation extent of Mo species at this MoO_3 content.

Ni–Mo/AZ catalysts. In Ni–Mo/AZ catalysts, the content of NiO in the γ-Al_2O_3 and zeolite phases is very close to the bulk composition (Fig. 7C). However, Mo tended to be associated with γ-Al_2O_3. The surface concentrations of both Ni and Mo in the calcined Ni–Mo/AZ catalysts reached a maximum at a $NiO/(NiO + MoO_3)$ ratio of 0.5 (Fig. 2), indicating that the surface species of Ni and Mo formed monolayers and were well dispersed when this ratio was <0.5. However, at a higher $NiO/(NiO + MoO_3)$ ratio, the Ni/Al ratio as detected by XPS was very high, indicating that bulk Ni oxide phases appeared, in agreement with the DRS and TEM observations. The surface concentrations of Ni and Mo species in the sulfided Ni–Mo/AZ catalysts also showed a maximum at $NiO/(NiO + MoO_3)$ ratios of 0.6 and 0.4 (Fig. 2), respectively, generally in agreement with their surface concentrations in the calcined catalysts. The sulfidation extent of both Ni and Mo species showed a broad maximum at a $NiO/(NiO + MoO_3)$ ratio of about 0.2–0.5 (Fig. 3B), which was correlated with the high surface concentrations and good dispersion of both Ni and Mo species. Thus, with an increase in the $NiO/(NiO + MoO_3)$ ratio to about 0.4, the surface concentrations of both Ni and Mo reached a maximum in the calcined catalysts, and the surface species was well dispersed and more easily sulfided to form a very dispersed so-called Ni–Mo–S phase under the sulfidation conditions (1); as a result, the HDS activity of DBT over Ni–Mo/AZ catalysts reached a prominent maximum at a $NiO/(NiO + MoO_3)$ ratio of 0.4.

Effects of USY Zeolite on HC and HDS Activity

Because the mixed support contained 60 wt% USY zeolite and 40 wt% γ-Al_2O_3, addition of the USY zeolite significantly improved the total acidity of the support and introduced a strong Brønsted acid site, compared with γ-Al_2O_3. As shown in Table 1, the HC activity of DPM generally increased with an increase in total acidity of the catalysts, but a quantitative correlation was difficult to establish. Thus, the HC activity of DPM over three series of Ni, Mo, and Ni–Mo catalysts supported on γ-Al_2O_3–USY zeolite was improved significantly compared with that of Ni–Mo/γ-Al_2O_3 catalyst, due to increasing acidity introduced by addition of USY zeolite.

The previous work indicated that the Ni/γ-Al_2O_3 catalyst has very low HDS activity; however, Mo/γ-Al_2O_3 catalyst has moderate HDS activity although it is far lower than that for Ni–Mo/γ-Al_2O_3 (Nishijima, private communication). Following addition of USY zeolite, Mo/γ-Al_2O_3–USY and particularly Ni/γ-Al_2O_3–USY catalysts had much higher HDS activity than the corresponding alumina-based catalysts. One possible explanation is that active metal phases (e.g., MoS_2 or Ni_3S_2 under the sulfidation conditions) and Brønsted acidity in USY zeolite synergistically enhanced HDS actiivity. By comparing Ni–Mo/γ-Al_2O_3–USY and Ni–Mo/γ-Al_2O_3 catalysts (15) that had identical nominal Ni and Mo loadings and that had been tested under identical reaction conditions, the HDS activity of DBT over the former was higher by about 10–15% than that over the latter. HDS activity of DBT depends on both HC and hydrogenation (HYD) activity. The general reaction path for HDS of DBT (e.g., over alumina-based catalysts) is as follows (1): DBT is decomposed to diphenyl by breaking the S–C bond (HC path) and to cyclohexybenzene by breaking benzene ring (HYD path). However, the reaction mechanisms for HDS of DBT over catalysts supported on γ-Al_2O_3–USY may be different. Unfortunately, our data are insufficient to address this mechanism due to limitations of the batch reactor used in this work. However, addition of USY zeolite into a conventional alumina-supported catalyst generally enhances HC activity but reduces HYD activity (5). Also the so-called Ni–Mo–S phase has much higher intrinsic HDS activity than MoS_2 or Ni_3S_2 (1). Thus, the synergistic effect of USY zeolite in sulfided Ni–Mo/γ-Al_2O_3–USY catalysts is not as significant as in sulfided Ni/γ-Al_2O_3–USY and Mo/γ-Al_2O_3–USY catalysts, and the HDS activity of DBT over Ni–Mo/γ-Al_2O_3–USY catalysts is also not much higher than that for the corresponding alumina-based catalyst.

CONCLUSIONS

1. The γ-Al_2O_3–USY zeolite support had much higher acidity than γ-Al_2O_3 alone. Addition of Ni and/or Mo to the support also improved the acidity. Consequently, γ-Al_2O_3–USY zeolite-supported Ni and/or Mo catalysts had much higher acidity and thus significantly higher HC activity than alumina-supported catalysts. The HC activity of DPM was generally proportional to the total acidity of the catalysts. However, there were two acid sites (one Lewis and one Brønsted) in the catalysts, and it was unclear which acid site contributed more to the HC activity of DPM.

2. Ni was essentially uniformly distributed in the catalysts, but Mo is preferentially associated with γ-Al_2O_3. Ni may occupy the surface vacancies and form monolayers on the surface of γ-Al_2O_3 and USY zeolite particles, or it may be incorporated into the supercavity and sodalite cage of the USY zeolite. Mo mainly occupied the surface vacancies and formed monolayers on the surface of γ-Al_2O_3, but it was only partially present on the surface of USY zeolite. However, when the content of NiO or MoO_3 was higher than about 5 mol%, the excess of Ni or Mo may have formed oxide aggregates on the surface of the support.

3. Both Ni and Mo catalysts supported on γ-Al_2O_3–USY zeolite showed high HDS activity, with a shallow maximum at about 5 mol% NiO and MoO_3. The activity was related to surface concentration, dispersion, and sulfidation extent, as well as acidity. Ni–Mo catalysts supported on γ-Al_2O_3–USY zeolite had higher HDS activity than γ-Al_2O_3-supported Ni–Mo catalyst, and they showed a prominent maximum at a $NiO/(NiO + MoO_3)$ ratio of about 0.4, similar to the γ-Al_2O_3-supported Ni–Mo catalyst. At this ratio, the total acidity was high, and the surface species of Ni and Mo were well dispersed and more easily sulfided. The primary active metal site for HDS of DBT over γ-Al_2O_3-supported Ni–Mo catalysts was probably the so-called Ni–Mo–S phase in γ-Al_2O_3. However, it cannot be excluded that a small amount of Ni and Mo may be redistributed into the supercavity of the USY zeolite during calcination, and the sulfided Ni–Mo species may also have partially contributed to the high HDS activity of DBT.

ACKNOWLEDGMENTS

D.L. acknowledges the Science and Technology Agency (STA) of Japan for the STA fellowship. We thank K. Masuda and Y. Kanda, Catalysts & Chemical Industry Ltd., Japan, for their technical assistance; Huifang Xu, University of New Mexico, for his assistance in TEM work; and J. W. Carey, Los Alamos National Laboratory, for his thorough review of the manuscript.

REFERENCES

1. Topsoe, H., Clausen, B. S., and Massoth, F. E., "Hydrotreating Catalysis: Science and Technology," p. 310. Spinger-Verlag, Berlin, 1996.
2. Maxwell, I. E., *Catal. Today* **1**, 385 (1987).
3. Mann, R. S., Sambi, I. S., and Khulbe, K. C., *Ind. Eng. Chem. Res.* **27**, 1788 (1988).
4. Harvey, T. G., and Pratt, K. C., *Appl. Catal.* **87**, 335 (1989).
5. Shimada, H., Sato, T., Yoshimura, Y., Hinata, A., Yoshitomi, S., Mares, A. C., and Nishijima, A., *Fuel Processing Technol.* **25**, 153 (1990).
6. Minja, R. J., and Ternan, M., *Energy Fuel* **5**, 117 (1991).
7. Yang, S. J., Chen, Y. W., and Li, C. P., *Appl. Catal. A* **115**, 59 (1994).
8. Yang, M. G., Nakamura, I., and Fujimoto, K., *Appl. Catal. A* **127**, 115 (1995).
9. Yang, M. G., Nakamura, I., and Fujimoto, K., *Appl. Catal. A* **144**, 221 (1996).
10. Yang, M. G., Nakamura, I., and Fujimoto, K., *Catal. Lett.* **39**, 33 (1996).
11. Yumoto, M., Usui, K., Watanabe, K., Idei, K., and Yamazaki, H., *Catal. Today* **35**, 45 (1997).
12. Li, D., Sato, T., Imamura, M., Shimada, H., and Nishijima, A., *J. Catal.* **170**, 357 (1997).
13. Portela, L., Grange, P., and Delmon, B., *J. Catal.* **156**, 243 (1995).
14. Kerkhof, F. P. J. M., and Moulijn, J. A., *J. Phys. Chem.* **83**, 1612 (1979).
15. Li, D., Sato, T., Imamura, M., Shimada, H., and Nishijima, A., *Appl. Catal. B* **16**, 255 (1998).
16. Xu, Y. D., Shu, Y. Y., Liu, S. T., Huang, J. S., and Guo, X. X., *Catal. Lett.* **35**, 233 (1995).
17. Galoisy, L., and Calas, G., *Am. Mineral.* **76**, 1777 (1991).
18. Rossman, G. R., Shannon, R. D., and Waring, R. K., *J. Solid State Chem.* **39**, 277 (1981).
19. White, W. B., McCarthy, G. J., and Scheetz, B. E., *Am. Mineral.* **56**, 72 (1971).
20. Liu, Z., and Chen, Y., *J. Catal.* **177**, 314 (1998).
21. Lepetit, C., and Che, M., *J. Phys. Chem.* **100**, 3137 (1996).
22. Schoonheydt, R. A., Roodhooft, D., and Leeman, H., *Zeolites* **7**, 412 (1987).
23. Li, D., Nishijima, A., and Morris, D. E., *J. Catal.* **182**, 339 (1999).
24. Jezlorowski, H., and Knözinger, H., *J. Phys. Chem.* **83**, 1166 (1979).
25. Williams, C. C., Ekerdt, J. G., Jehng, J. M., Hardcastle, F. D., and Wachs, I. E., *J. Phys. Chem.* **95**, 8791 (1991).
26. Spanos, N., Vordonis, L., Kordulis, C., and Lycourghiotis, A., *J. Catal.* **124**, 301 (1990).
27. Vordonis, L., Spanos, N., Koutsoukos, P. G., and Lycourghiotis, A., *Langmuir* **8**, 1736 (1992).
28. Spanos, N., and Lycourghiotis, A., *J. Colloid Interface Sci.* **171**, 306 (1995).
29. Spanos, N., and Lycourghiotis, A., *J. Catal.* **147**, 57 (1994).
30. Cheah, S. F., Brown G. E., and Parks, G. A., *J. Colloid Interface Sci.* **208**, 110 (1998).
31. Bargar, J. R., Brown, G. E., and Parks, G. A., *Geochim. Cosmochim. Acta* **61**, 2639 (1997).